Flow (2023), **3** E26
doi:10.1017/flo.2023.22

FLOW CAMBRIDGE UNIVERSITY PRESS

RESEARCH ARTICLE

Benefits of controlled inclination for contactless transport by squeeze-film levitation

Sankaran Ramanarayanan[1],* and Antonio L. Sánchez[1]

[1]Department of Mechanical and Aerospace Engineering, University of California San Diego, La Jolla, CA 92093-0411, USA
*Corresponding author. E-mail: sramanar@ucsd.edu

Received: 31 March 2023; **Revised:** 13 June 2023; **Accepted:** 11 July 2023

Keywords: Squeeze-film levitation; Lubrication theory; General fluid mechanics; Propulsion systems; Locomotion

Abstract

Developed in this paper is a theoretical description of the fluid flow involved in contactless transport systems that operate using squeeze-film levitation. Regular perturbation methods are employed to solve the appropriate Reynolds equation that governs the viscous, compressible flow of air in the slender film separating the oscillator and the levitated object. The resulting reduced formulation allows efficient computation of the time-averaged levitation force and moment induced by fluid pressure, as well as the accompanying quasistatic thrust force that accounts additionally for shear stresses. Investigated, in particular, is the possibility of combining two distinct methods of thrust generation that have been experimentally demonstrated in previous studies – (i) inclination of the levitated body and (ii) generation of asymmetrical flexural deformations, such as travelling waves, on the oscillator surface – the latter of which is shown to allow a transition from the typically repulsive levitation force to one that is attractive. Computations reveal that systematic control of the inclination angle can provide significant performance benefits for squeeze-film transport systems. In the case of attractive levitation, the amount of improvement that can be obtained appears to correlate closely with the degree of lateral asymmetry exhibited by the flexural oscillations.

Impact Statement

Contactless transportation using squeeze-film levitation is of rapidly growing interest in applications such as the assembly line manufacturing of touch-sensitive objects and soft-robotic locomotion over complex terrain. Achieving lateral mobility in levitation systems has typically required incorporation of multiple oscillation sources, which consume substantial energy while generating thrust forces and transport speeds that are inadequate for large-scale, practical application. The results of the present analysis demonstrate that much greater thrust can be generated by controlling systematically the inclination angle of an object levitated by repulsive or attractive pressure forces, for instance, through active control of the centre of mass of a self-levitating robot. The generality and computational efficiency of this mathematical formulation make it a versatile tool for guiding the design, optimization and closed-loop control of next-generation squeeze-film transport systems.

1. Introduction

A typical squeeze-film levitation (SFL) system, as cartooned in figure 1(*a*), consists of two rigid objects with parallel surfaces that are separated by a slender layer of air, the 'squeeze film'. High-frequency

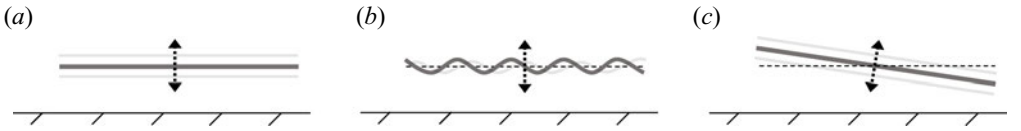

Figure 1. *(a) A conventional squeeze-film levitation system can be modified to generate thrust by (b) excitation of propagating-wave surface deformations or (c) inclination of the oscillator surface.*

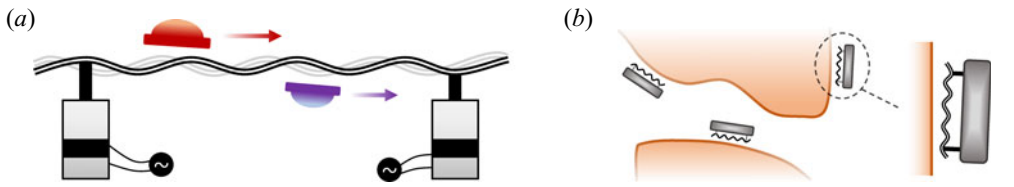

Figure 2. *Proposed applications of squeeze-film transport: (a) contactless assembly line conveyance using both repulsion (red) and attraction (blue), and (b) soft-robotic locomotion over complex terrain.*

oscillation of either object along an axis perpendicular to the surfaces generates pulsating airflow in the film that yields a strong, steady, repulsive pressure force between the two objects. This phenomenon has been exploited to design gas-lubricated bearings (Salbu, 1964; Shi, Feng, Hu, Zhu, & Cui, 2019) and levitation devices that exhibit large load capacities, as demonstrated, for example, by Zhao (2010), who developed an ultrasonic oscillator with a small surface diameter of 5 cm that generated 115 N (≈11.7 kgf) of repulsion.

Squeeze-film levitation systems are typically operated at a frequency that corresponds to one of the resonant bending modes of the oscillating assembly. Active feedback control of the excitation signal has been implemented to account for slight, unpredictable drifts of the natural frequency (Ilssar, Bucher, & Flashner, 2017). The drastic increase in the amplitude of oscillations near resonance magnifies substantially the repulsive levitation force (Li, Liu, & Ding, 2014; Matsuo, Koike, Nakamura, Ueha, & Hashimoto, 2000). The effective flexural amplitude can be improved by reducing the stiffness of the oscillator through careful selection of material(s) (Shi, An, Feng, Guo, & Liu, 2018; Wang & Au, 2013) and geometry (Stolarski, Gawarkiewicz, & Tesch, 2015).

Under a limited range of operating conditions – namely, for surfaces with millimetric characteristic dimensions or oscillation frequencies as low as several hundred hertz – this steady force has been observed to transition from strong repulsion to weak suction of less than 1 gf (Andrade, Ramos, Adamowski, & Marzo, 2020; Sadayuki, 2002; Takasaki, Terada, Kato, Ishino, & Mizuno, 2010; Yoshimoto, Shou, & Somaya, 2013). Recent experiments have shown that this minor attractive load capacity is magnified a thousand fold when the stiffness of the oscillator is reduced substantially to provide pronounced flexural deformations that may be subject to non-negligible fluid–structure coupling (Colasante, 2015; Weston-Dawkes et al., 2021). A preliminary theoretical analysis (Ramanarayanan & Sánchez, 2022) indicated that the range of operating conditions under which attraction occurs, as well as the magnitude of the resulting force, grows substantially with the wavenumber of oscillation, i.e. with the number of nodes in the associated standing wave, although effects of coupling remain to be understood.

Proposed applications of SFL include, primarily, assembly line manufacturing of touch-sensitive items, such as surface-mount devices for circuit boards (Andrade et al., 2020) and glass substrates to be installed in liquid-crystal displays (Hatanaka, Koike, Nakamura, Ueha, & Hashimoto, 1999), and load-carrying ‘soft’ robots that can travel over multifarious terrains (Weston-Dawkes et al., 2021); see figure 2 for a rudimentary visualization of each. Pursuant of these applications, a number of methods have been proposed to modify the basic SFL configuration to produce also lateral forces, as reviewed in the following paragraphs.

https://doi.org/10.1017/flo.2023.22 Published online by Cambridge University Press

The earliest of these is the excitation of travelling-wave deformations of the oscillator, as diagrammed in figure 1(*b*), which generates steady, asymmetrical fluid shear on the bounding surfaces of the squeeze film. This method has been applied to develop rail-transport systems that levitate repulsively objects with masses of the order of 10–100 grams and displace them with speeds of the order of 10 cm s^{-1} (Ide, Friend, Nakamura, & Ueha, 2007; Sadayuki, 2002; Yin, 2008). Experimenters have also designed self-levitating mobile robots with comparable masses that can produce thrust forces of the order of 10 mN (Feng, Liu, & Cheng, 2015; Koyama, Nakamura, & Ueha, 2007). The wave-generation methods employed in these experiments involve two spatially separated oscillators attached to a platform (Syuhri, 2022). Of great concern has been the purity of the travelling wave generated on the finite platform – which is limited practically by reflection at free boundaries and points of attachment, since the resulting interference may critically reduce the thrust force (Feng et al., 2015). Ameliorative solutions include 'impedance matching', where one of the oscillators acts as a passive absorber through piezoelectric energy dissipation (Hariri, Bernard, & Razek, 2013; Sadayuki, 2002), and 'two-mode excitation', where the two oscillators operate out of phase at a critical frequency that results in a favourable superposition of two consecutive resonant modes of the platform (Loh & Ro, 2000; Tomikawa, Adachi, Hirata, Suzuki, & Takano, 1990). Active feedback control using the latter method has been claimed to provide nearly perfect travelling waves (Ghenna, Giraud, Giraud-Audine, Amberg, & Lemaire-Semail, 2015; Giraud, Giraud-Audine, Amberg, & Lemaire-Semail, 2014).

Three prominent alternative methods of transport have been proposed in recent years. The first relies on the steady shear force caused by the asymmetrical fluid streaming that occurs when a levitated object is misaligned with a finite parallel surface (Yano, Aoyagi, Tamura, & Takano, 2011). This so-called 'restoring force' is exploited by assembling an array of oscillators and controlling carefully the amplitude of each such that fluid shear conveys a levitated object along the array. Notable limitations of this method include the need for multiple oscillators, whose number and/or size must grow with the desired transport distance, and the apparent inapplicability to robotic locomotion.

Chen, Gao, Pan, and Guo (2016) proposed a remarkable method more amenable to robotic applications – simultaneous generation of linear and rotational oscillations of a platform using a pair of independently excited piezoelectric elements, the resonant frequencies of the two oscillation modes matched using computer-aided design. In principle, if the modes are driven exactly out of phase, the oscillations should resemble a travelling wave with very large wavelength. The authors report an optimal phase shift of $\approx 25^\circ$, which allowed a roughly 20 g robot to travel at 2.25 cm s^{-1} and generate 30 mN of static thrust.

The third and most recent alternative, proposed by Wei, Shaham, and Bucher (2018), involves inclination of the levitated object, as exemplified in figure 1(*c*), which would tilt the levitation force vector to provide a relatively small lateral component. This method seems particularly attractive for implementation on mobile robots, simply through active control of the on-board mass distribution. Although the robustness and stability of steady-state transport are yet to be investigated rigorously for this method, Wei et al. (2018) claim that it may yield substantial advantages in versatility, load capacity and controllability.

A unifying factor among the literature cited above is the focus on repulsive levitation. To the best of our knowledge, controlled transport using attraction is yet to be studied. Explored in this paper is the prospect of combining the distinct thrust-generation mechanisms of (i) travelling-wave deformations and (ii) controlled surface inclination. Results of a rigorous fluid-flow analysis indicate that both the thrust and the levitation force generated by an asymmetrical SFL system, whether the latter be repulsive or attractive, can be improved substantially through methodical adjustment of the tilting angle.

The remainder of this paper is organized as follows. Outlined in § 2 is the proposed fluid-dynamic problem that represents a generic squeeze-film system involving arbitrary flexural oscillations and a variable tilt angle. The reduced conservation equations governing fluid flow in the slender air layer are presented, followed by the introduction of appropriately rescaled dimensionless variables. An asymptotic solution is derived in § 3 and integral expressions are provided for the steady

https://doi.org/10.1017/flo.2023.22 Published online by Cambridge University Press

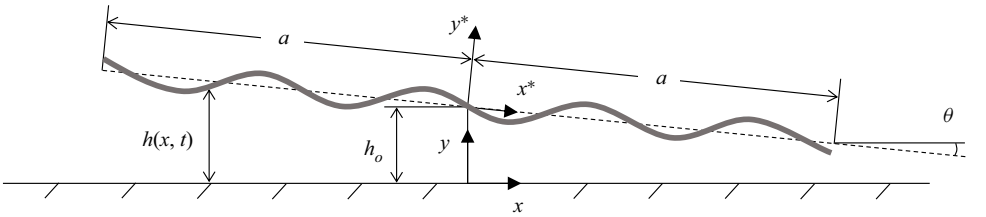

Figure 3. *A generic squeeze-film transport system: a levitated plate undergoing flexural oscillation is tilted at an angle θ with respect to a nearby wall and propelled to the right by fluid stresses beneath.*

thrust force, the levitation force and the associated centre of pressure. These levitation metrics are visualized in § 4 for a variety of relevant transport configurations. The paper concludes with a discussion of possible applications of the developed formulation in system design, optimization and control.

2. Problem definition

2.1. Preliminary considerations

Consider, as a relevant canonical configuration, the planar SFL system represented in figure 3, where a plate of undeformed length $2a$ levitates and translates above an infinitely long horizontal wall. In its undeformed state, the plate is tilted at an angle θ with respect to the wall, and its centre is separated from the wall by a time-averaged distance h_o. The plate undergoes time-harmonic, flexural oscillations that are described by the equation $y^* = b\,Re\{W(x^*/a)\,\mathrm{e}^{\mathrm{i}\omega t}\}$, where (x^*, y^*) specifies the depicted rotated coordinate system attached to the plate centre, b and ω denote, respectively, the characteristic amplitude and angular frequency of oscillation, and W is a dimensionless function that defines the waveform. For instance, the cases $W = \cos(2\pi x^*/a)$ and $W = \exp(-2\,\mathrm{i}\pi x^*/a)$ represent, respectively, standing waves and forward-travelling waves of wavelength a.

The local pressure, temperature, density and viscosity of the oscillating gas inside the film are denoted, respectively, by p, T, ρ and μ. The corresponding values of those properties in the unperturbed surroundings are denoted with the subscript 'a'; for instance, p_a denotes the ambient pressure.

For typical SFL systems (Matsuo et al., 2000; Yoshimoto et al., 2013; Zhao, 2010),

(i) the squeeze film is slender, $h_o \ll a$, whereby the tilt angle is small, $\theta \sim h_o/a \ll 1$;
(ii) the characteristic wavelength of the flexural oscillations is comparable to a, whereby
(iii) any lateral displacement Δx^* of points on the deforming plate surface is negligible; and
(iv) the transport speed u_t is negligibly small (Ide et al., 2007) compared with the characteristic speed u_s of steady gaseous streaming in the film: $u_t \ll u_s \sim (b/h_o)^2\omega a$ (Ramanarayanan, Coenen, & Sánchez, 2022).

Assumptions (i) and (ii) allow application of the slender-flow approximation (Ramanarayanan et al., 2022) to model gas flow in the film. Due to (iii) and (iv), the only non-trivial boundary condition to be imposed for the flow velocity stems from the transverse motion of the plate surface, which can now be expressed with use of the simplified equation

$$y = h(x,t) = h_o - x\theta + b\,Re\{W(x/a)\,\mathrm{e}^{\mathrm{i}\omega t}\} \quad \text{for } -a \le x \le a, \tag{2.1}$$

where (x, y) denotes a coordinate system whose origin travels along the wall (see figure 3), with x coincident to the wall and y denoting the distance to the plate centre. The assumption of small angles $\theta \ll 1$ introduces relative errors of order θ^2 for the terms representing steady tilt and unsteady flexure.

https://doi.org/10.1017/flo.2023.22 Published online by Cambridge University Press

The levitation force, defined as the vertical component of the time-averaged aerodynamic force acting on the plate (per unit length perpendicular to the plane of motion), can then be expressed as

$$\langle \mathcal{F}_L \rangle = \int_{-a}^{a} \langle p - p_a \rangle \, \mathrm{d}x, \tag{2.2}$$

and the associated thrust force – the horizontal component – can be expressed as

$$\langle \mathcal{F}_T \rangle = \int_{-a}^{a} (\langle p - p_a \rangle \theta - \langle \mu \partial u / \partial y \rangle|_{y=h}) \, \mathrm{d}x, \tag{2.3}$$

both with relative errors of order $(h_o/a)^2 \sim \theta^2$. The angled brackets in the definitions above denote the time average of a time-dependent quantity over one period of oscillation, $\langle \star \rangle = (\omega/2\pi) \int_{t^*}^{t^*+2\pi/\omega} \star \, \mathrm{d}t$.

In addition, the levitation moment about the plate centre and the associated centre of steady pressure can be expressed as

$$\langle \mathcal{M} \rangle = \int_{-a}^{a} \langle p - p_a \rangle x \, \mathrm{d}x \quad \text{and} \quad x_{csp} = \frac{\langle \mathcal{M} \rangle}{\langle \mathcal{F}_L \rangle}, \tag{2.4a,b}$$

with the same level of accuracy. Note that, due to the simplifications employed, the quasistatic transport problem defined above also describes, in principle, systems such as those depicted in figure 2(*a*), where a rigid object with a flat surface (of length 2*a*) is transported over a flexurally oscillating rail.

2.2. The lubrication approximation

As shown by Melikhov, Chivilikhin, Amosov, and Jeanson (2016) and Ramanarayanan et al. (2022), the flow dynamics in the thin air layer of a squeeze-film system is characterized by three principal time scales – that of the driving oscillations $t_o = \omega^{-1}$, viscous diffusion across the film $t_v = h_o^2/(\mu_a/\rho_a)$ and acoustic pressure equilibration along the film $t_a = a/\sqrt{p_a/\rho_a}$ – which enter in the theoretical description through two non-dimensional parameters, the relevant Stokes number $\mathcal{S} = t_v/t_o$ (or, equivalently, the associated Womersley number $S^{1/2}$) and a compressibility number $C = t_a/t_o$. As shown by Taylor and Saffman (1957), the description simplifies in configurations for which $t_v \ll t_o$, whereby inertial forces are negligibly weak compared with viscous shear. In the associated lubrication limit $\mathcal{S} \ll 1$, the three time scales are found to enter through a single governing fluidic parameter

$$\sigma = \frac{12C^2}{\mathcal{S}} = \frac{12t_a^2}{t_o t_v} = \frac{12\mu_a \omega a^2}{p_a h_o^2} \sim 1, \tag{2.5}$$

where the factor of 12 is included for consistency with the classical definition. Often referred to as the 'squeeze number', σ effectively represents the combined effects of gaseous compressibility and viscous shear within the film. Solution for the case of parallel walls ($\theta = 0$) with uniform oscillation amplitude ($W = 1$) has revealed that the air near the centre of the film is entrapped due to viscous resistance, and its nonlinear response to time-harmonic compression and expansion provides the steady repulsive pressure force $\langle \mathcal{F}_L \rangle$ (Langlois, 1962; Salbu, 1964). The extent of this central region and, hence, the magnitude of the force, grows monotonically with increasing values of σ. On the other hand, as $\sigma \to 0$ and the system becomes weakly nonlinear, the force vanishes, proportional to σ^2 (Ramanarayanan et al., 2022).

While quantifying the effects of local and convective fluid acceleration affords higher accuracy in the computation of the levitation force for a wider range of operating parameters (Li, Cao, Liu, & Ding, 2010; Melikhov et al., 2016; Minikes & Bucher, 2006), the lubrication limit has been shown to provide excellent agreement with experimental measurements for systems with small mean distances $h_o \ll \sqrt{\mu_a/(\rho_a \omega)}$, those that satisfy $t_v \ll t_o$, for which the strongest forces – both repulsive and attractive – are expected to occur (Ramanarayanan & Sánchez, 2022; Salbu, 1964; Zhao, 2010). Therefore, in the following analysis, the classical compressible lubrication approximation ($t_v/t_o \sim t_a^2/t_o^2 \ll 1$) will be employed to describe

https://doi.org/10.1017/flo.2023.22 Published online by Cambridge University Press

rigorously the family of transport systems schematized in figure 3. The mathematical formulation derived below may be readily extended in the future to address the general viscoacoustic limit ($t_v/t_o \sim t_a/t_o \sim 1$) by following the methods of Ramanarayanan et al. (2022), although quantification of inertial effects would severely limit the degree of analytical development possible.

The fluid flow in asymmetrical SFL systems has been studied previously for two limiting cases that correspond to the canonical transport mechanisms drawn in figures 1(*b*) and 1(*c*). For the latter, where $W = 1$ and $\theta \neq 0$, DiPrima (1968) outlined an asymptotic computation of the time-dependent film pressure under the assumption of a known, non-negligible transport speed. A verified numerical model, developed by Wei et al. (2018) using the ANSYS CFX software, provided preliminary insights into the correlation between the tilt angle and the thrust force contributed by fluid shear. For the former, where $\theta = 0$ and $W = W(\xi)$, Minikes, Bucher, and Haber (2004) computed analytically the quasistatic thrust force in the case of pure travelling-wave oscillations with variable wavenumber. Feng et al. (2015) presented a numerical investigation of the problem for imperfect travelling waves, demonstrating the adverse effect of impurity on the thrust force. The utilized model accounted rigorously for effects of local fluid acceleration and estimated the additional drag force induced by fluid shear on the exposed plate surface.

Two notable treatments of the generic problem depicted in figure 3 must be mentioned here. Minikes and Bucher (2003) presented a formulation similar to that of Feng et al. (2015) but computed additionally the contribution of steady overpressure to the thrust in the presence of inclination, quantifying the adverse effect of the impurity of travelling waves on the terminal transport velocity. Li, Liu, and Zhang (2017) addressed the stability of transport systems to disturbances in the tilt angle θ, using a model that accounts for fluid inertia but neglects the fundamental role of gaseous compressibility. They discovered a steady restoring moment that increases in magnitude with the inclination angle. However, (i) systematic modulation of thrust by controlling the inclination and (ii) achievement of transport with attractive levitation were beyond the scopes of these studies, and are explored below.

2.3. Conservation equations governing airflow in the squeeze film

Under the limit $t_v \ll t_o$, the Navier–Stokes equations (continuity and conservation of momentum in the lateral and transverse directions) and the thermal equation of state for an ideal gas reduce, respectively, to

$$\frac{\partial \rho}{\partial t} + \frac{\partial (\rho u)}{\partial x} + \frac{\partial (\rho v)}{\partial y} = 0, \quad \mu_a \frac{\partial^2 u}{\partial y^2} = \frac{\partial p}{\partial x}, \quad \frac{\partial p}{\partial y} = 0 \quad \text{and} \quad \frac{p}{p_a} = \frac{\rho}{\rho_a}, \tag{2.6a–d}$$

with relative errors of order $(h_o/a)^2$. In deriving the above equations, it has been assumed for simplicity that both the plate and wall surfaces are held at the ambient temperature T_a, whereby the conservation of energy implies that $T = T_a$ everywhere in the film. As a result, the dynamic viscosity can be considered uniform as well, $\mu(T) = \mu_a$ (Chapman & Cowling, 1990). Detailed discussions of these equations, which comprise the isothermal compressible lubrication limit, are presented by Taylor and Saffman (1957), Langlois (1962) and Ramanarayanan et al. (2022).

In pursuit of a reduced dimensionless formulation of the problem, we introduce the appropriately rescaled flow variables $\xi = x/a$, $Y = y/h_o$, $\tau = \omega t$, $U = u/(\varepsilon \omega a)$, $V = v/(\varepsilon \omega h_o)$ and $P = (p - p_a)/(\varepsilon \sigma p_a/12) = (\rho - \rho_a)/(\varepsilon \sigma \rho_a/12)$, where the quantity σ is defined in (2.5). Note that the characteristic scales for the variations of pressure and density follow from straightforward order-of-magnitude analyses of the lateral momentum equation and the equation of state, respectively. Upon defining additionally a rescaled inclination angle $\varphi = \theta/(h_o/a)$, the plate position (2.1) can be rewritten as

$$\frac{h}{h_o} = H(\xi, \tau) = 1 - \varphi \xi + \varepsilon \, Re\{W(\xi)\, \mathrm{e}^{\mathrm{i}\tau}\}, \quad \text{where} \left| \varphi = \frac{\theta}{h_o/a} \right| \leq 1 - \varepsilon, \tag{2.7}$$

with relative errors of order θ^2 and $\varepsilon\theta^2$ stemming, respectively, from the terms describing tilt and flexure.

https://doi.org/10.1017/flo.2023.22 Published online by Cambridge University Press

Substituting these definitions into the lateral momentum and continuity equations provides

$$\frac{\partial^2 U}{\partial Y^2} = \frac{\partial P}{\partial \xi} \quad \text{and} \quad \frac{\sigma}{12}\frac{\partial P}{\partial \tau} + \frac{\partial}{\partial \xi}\left[\left(1 + \varepsilon\frac{\sigma}{12}P\right)U\right] + \frac{\partial}{\partial Y}\left[\left(1 + \varepsilon\frac{\sigma}{12}P\right)V\right] = 0, \tag{2.8a,b}$$

respectively, where $P = P(\xi, \tau)$ due to the transverse momentum equation. The above system of equations is subject to non-slip and non-penetration conditions on the bounding walls,

$$U = V = 0 \quad \text{at } Y = 0 \quad \text{and} \quad U = V - \varepsilon^{-1}\partial H/\partial \tau = 0 \quad \text{at } Y = H, \tag{2.9a,b}$$

expressed here with errors of order θ^2.

Upon integrating the momentum equation twice in the Y direction and applying the conditions $U(Y = 0) = U(Y = H) = 0$, we obtain the quasisteady Poiseuille velocity profile

$$U(\xi, Y, \tau) = \frac{1}{2}\frac{\partial P}{\partial \xi}Y(Y - H), \tag{2.10}$$

involving the time-varying lateral pressure gradient $\partial P/\partial \xi$. Substituting this result into the continuity equation, integrating across the film, applying the conditions $V(Y = 0) = V(Y = H) - Re\{W(\xi)\,\mathrm{i}\,\mathrm{e}^{\mathrm{i}\tau}\} = 0$ and simplifying with use of the Leibniz integral rule yields the relevant Reynolds equation

$$\sigma\frac{\partial (PH)}{\partial \tau} - \frac{\partial}{\partial \xi}\left[H^3\left(1 + \varepsilon\frac{\sigma}{12}P\right)\frac{\partial P}{\partial \xi}\right] + 12\,Re\{W(\xi)\,\mathrm{i}\,\mathrm{e}^{\mathrm{i}\tau}\} = 0. \tag{2.11}$$

Two boundary conditions for $P(\xi, \tau)$ are required to close the problem defined by (2.7), (2.10) and (2.11).

Previous studies have shown that the pressure in the squeeze film relaxes to its ambient value across small, non-slender peripheral regions that extend distances $|\Delta \boldsymbol{x}|$ of order $h_o \ll a$ beyond the edges $\xi = \pm 1$ (Ramanarayanan et al., 2022; Yoshimoto et al., 2013). Due to the associated disparity of scales, the characteristic variations of pressure across these peripheries are smaller than those along the film – where $\Delta x \sim a$ – by order h_o/a. For arbitrary order-unity values of the relative amplitude $\varepsilon \lesssim 1$, (2.11) can therefore be readily solved using numerical methods when supplemented by the simple boundary conditions $P(\xi = \pm 1) = 0$, which introduce small relative errors of $O(h_o/a \ll 1)$. Finite-difference solutions of the strongly nonlinear Reynolds equation have displayed excellent agreement with experimental results for operating conditions that fall under the lubrication limit $t_v \ll t_o$ (Salbu, 1964; Zhao, 2010). In the present study, numerical integration of (2.11) was performed using a straightforward central-space, forward-Euler scheme for the purpose of verifying the asymptotic solution derived below. Instructions for implementing the algorithm, as well as discussions regarding its stability, accuracy and computational efficiency, are provided by Michael (1963).

3. Asymptotic solution

To allow efficient analytical reduction of the problem at hand, it will be assumed that the oscillation amplitude $\Delta y^* = b$ is small relative to the mean thickness of the air layer, i.e. $b \ll h_o$, which allows asymptotic solution using the relative amplitude

$$\varepsilon = \frac{b}{h_o} \ll 1, \tag{3.1}$$

as the small perturbation parameter. Despite operating near resonance, typical SFL systems exhibit diminutive amplitudes of the order of $b = 10\ \mu\mathrm{m}$ (Andrade et al., 2020; Ide et al., 2007; Zhao, 2010), whereby an asymptotic solution can provide reasonable accuracy as long as the film thickness h_o is relatively large (Ramanarayanan & Sánchez, 2022). On the other hand, the strongly repulsive forces that are generated at close range ($h_o \sim b$) are best quantified using a numerical solution of the Reynolds

https://doi.org/10.1017/flo.2023.22 Published online by Cambridge University Press

equation (Zhao, 2010), as described in § 2.3, or a direct numerical simulation using the full Navier–Stokes equations (Andrade et al., 2020; Yoshimoto et al., 2013).

Under the limit of small relative amplitudes $\varepsilon \ll 1$, the required boundary conditions for the fluid pressure at the film edges must be developed carefully. We begin by introducing perturbation expansions for the pressure and lateral flow velocity component,

$$\left.\begin{aligned} P &= P_0 + \varepsilon P_1 + \cdots, \\ U &= U_0 + \varepsilon U_1 + \cdots. \end{aligned}\right\} \tag{3.2}$$

As shall be shown in § 3, substitution of this expansion into (2.11) leads to an equation that is linear at leading order. Thus, the first term in each expansion varies harmonically with time and yields no contribution to the time-averaged levitation forces and moment, whose evaluation consequently requires the computation of first-order corrections. Due to the disparity of spatial scales between the slender film and the small non-slender regions surrounding its edges, discussed below (2.11), the leading-order pressure accepts simple relaxation conditions: $P_0(\xi = \pm 1) = 0$. However, determining the corresponding conditions for P_1 requires, in principle, establishing a formal asymptotic relationship between the two small parameters ε and h_o/a, and systematically matching (Lagerstrom, 1988) with the local asymptotic expansions for the pressure in the two non-slender peripheries (Ramanarayanan et al., 2022). Fortunately, for $\varepsilon \ll 1$, the reduced conservation equations that govern the peripheries under the lubrication limit are linear in the first approximation (Ramanarayanan et al., 2022). The peripheral pressure variations correspondingly exhibit a zero time average, whereby relaxation conditions can be imposed for the time-averaged first-order pressure, $\langle P_1 \rangle(\xi = \pm 1) = 0$. While these conditions do not allow computation of the time dependence of $P_1(\xi, \tau)$, they are sufficient to solve for the desired steady levitation metrics (2.2)–(2.4*a*,*b*).

Substituting the expression for $H(\xi, \tau)$ given in (2.7) along with the first two terms of the pressure expansion (3.2) into the Reynolds equation (2.11) yields

$$\begin{aligned} &\sigma \frac{\partial}{\partial \tau}\left[(P_0 + \varepsilon P_1)(1 - \varphi\xi + \varepsilon\, Re\{W\, \mathrm{e}^{\mathrm{i}\tau}\})\right] + 12\, Re\{W\, \mathrm{i}\, \mathrm{e}^{\mathrm{i}\tau}\} \\ &\quad - \frac{\partial}{\partial \xi}\left[(1 - \varphi\xi + \varepsilon\, Re\{W\, \mathrm{e}^{\mathrm{i}\tau}\})^3 \left[1 + \varepsilon \frac{\sigma}{12}(P_0 + \varepsilon P_1)\right] \frac{\partial}{\partial \xi}(P_0 + \varepsilon P_1)\right] = 0, \end{aligned} \tag{3.3}$$

which is to be solved to determine $P(\xi, \tau)$ with small errors of $O(\varepsilon^2)$ and $O(h_o^2/a^2 \sim \theta^2)$.

The horizontal velocity distribution $U(\xi, Y, \tau)$ can, in turn, be found with the same level of accuracy using the expanded form of (2.10),

$$U_0 + \varepsilon U_1 = \frac{1}{2} \frac{\partial}{\partial \xi}(P_0 + \varepsilon P_1) Y [Y - (1 - \varphi\xi + \varepsilon\, Re\{W\, \mathrm{e}^{\mathrm{i}\tau}\})]. \tag{3.4}$$

3.1. Leading-order solution

Collecting terms of order unity in (3.3) leads to the linear equation

$$\sigma(1 - \varphi\xi) \frac{\partial P_0}{\partial \tau} - \frac{\partial}{\partial \xi}\left[(1 - \varphi\xi)^3 \frac{\partial P_0}{\partial \xi}\right] + 12\, Re\{W(\xi)\, \mathrm{i}\, \mathrm{e}^{\mathrm{i}\tau}\} = 0, \tag{3.5}$$

which can be solved using the method of separation of variables. Upon substituting the ansatz

$$P_0 = Re\{\Pi(\xi)\, \mathrm{e}^{\mathrm{i}\tau}\}, \tag{3.6}$$

https://doi.org/10.1017/flo.2023.22 Published online by Cambridge University Press

(3.5) reduces to the equidimensional ordinary differential equation

$$\frac{\mathrm{d}^2\Pi}{\mathrm{d}\xi^2} - \frac{3\varphi}{1-\varphi\xi}\frac{\mathrm{d}\Pi}{\mathrm{d}\xi} - \frac{\sigma\,\mathrm{i}}{(1-\varphi\xi)^2}\Pi = 12\,\mathrm{i}\frac{W(\xi)}{(1-\varphi\xi)^3}, \quad \text{with } \Pi(\xi=\pm1)=0. \tag{3.7}$$

Solution by the method of variation of parameters gives the reduced pressure distribution

$$\Pi(\xi) = \frac{6\,\mathrm{i}}{\alpha\varphi(1-\varphi\xi)}\left[L(\xi) - \frac{1-[(1+\varphi)/(1-\varphi\xi)]^{2\alpha}}{1-[(1+\varphi)/(1-\varphi)]^{2\alpha}}\left(\frac{1-\varphi\xi}{1-\varphi}\right)^{\alpha} L(1)\right], \tag{3.8}$$

expressed in terms of the parameter

$$\alpha = \sqrt{1+\frac{\sigma\,\mathrm{i}}{\varphi^2}}, \tag{3.9}$$

and the integral operator

$$L(\xi) = \frac{\int_{-1}^{\xi} W(\tilde{\xi})(1-\varphi\tilde{\xi})^{\alpha-1}\,\mathrm{d}\tilde{\xi}}{(1-\varphi\xi)^{\alpha}} - (1-\varphi\xi)^{\alpha}\int_{-1}^{\xi}\frac{W(\tilde{\xi})}{(1-\varphi\tilde{\xi})^{\alpha+1}}\,\mathrm{d}\tilde{\xi}, \tag{3.10}$$

where $\tilde{\xi}$ is a dummy integration variable. The reduced pressure gradient $\Pi' = \mathrm{d}\Pi/\mathrm{d}\xi$ is given by

$$\Pi'(\xi) = \frac{6\,\mathrm{i}}{\alpha\varphi(1-\varphi\xi)^2}\left[\tilde{L}(\xi) + \frac{1-\alpha-(1+\alpha)[(1+\varphi)/(1-\varphi\xi)]^{2\alpha}}{1-[(1+\varphi)/(1-\varphi)]^{2\alpha}}\left(\frac{1-\varphi\xi}{1-\varphi}\right)^{\alpha} L(1)\right], \tag{3.11}$$

involving the additional integral operator

$$\tilde{L}(\xi) = (1-\alpha)(1-\varphi\xi)^{\alpha}\int_{-1}^{\xi}\frac{W(\tilde{\xi})}{(1-\varphi\tilde{\xi})^{\alpha+1}}\,\mathrm{d}\tilde{\xi} - (1+\alpha)\frac{\int_{-1}^{\xi} W(\tilde{\xi})(1-\varphi\tilde{\xi})^{\alpha-1}\,\mathrm{d}\tilde{\xi}}{(1-\varphi\xi)^{\alpha}}. \tag{3.12}$$

Finally, collecting terms of order unity in (3.4) gives the leading-order horizontal velocity distribution

$$U_0 = \frac{\partial P_0}{\partial\xi}\frac{Y(Y-1+\varphi\xi)}{2}, \tag{3.13}$$

expressed here in terms of the gradient of the known leading-order pressure P_0, given in (3.6).

Since P_0 varies harmonically with time and, thus, exhibits a zero time average, i.e. $\langle P_0\rangle = 0$, evaluation of the steady levitation metrics (2.2)–(2.4*a*,*b*) requires computation of first-order corrections.

3.2. First-order corrections

Collecting terms of order ε in (3.3) and taking the time average gives

$$3(1-\varphi\xi)^2\left\langle Re\{W\,\mathrm{e}^{\mathrm{i}\tau}\}\frac{\partial P_0}{\partial\xi}\right\rangle + \frac{\sigma}{12}(1-\varphi\xi)^3\left\langle P_0\frac{\partial P_0}{\partial\xi}\right\rangle + (1-\varphi\xi)^3\left\langle\frac{\partial P_1}{\partial\xi}\right\rangle = 0, \tag{3.14}$$

which can be integrated subject to the boundary conditions $\langle P_1\rangle(\xi=\pm1)=0$ to give

$$\langle P_1\rangle(\xi) = \frac{(1-\varphi)^2}{4\varphi}\left[\left(\frac{1+\varphi}{1-\varphi\xi}\right)^2 - 1\right]\int_{-1}^{1} G(\xi)\,\mathrm{d}\xi - \int_{-1}^{\xi} G(\tilde{\xi})\,\mathrm{d}\tilde{\xi}, \tag{3.15}$$

where

$$G(\xi) = \left\langle\frac{\partial P_0}{\partial\xi}\left(\frac{3}{1-\varphi\xi}Re\{W\,\mathrm{e}^{\mathrm{i}\tau}\} + \frac{\sigma}{12}P_0\right)\right\rangle. \tag{3.16}$$

https://doi.org/10.1017/flo.2023.22 Published online by Cambridge University Press

Upon substituting the definition of the leading-order pressure (3.6) and applying the identity

$$\langle Re\{\mathcal{A}(\xi)\,\mathrm{e}^{\mathrm{i}\tau}\}\,Re\{\mathcal{B}(\xi)\,\mathrm{e}^{\mathrm{i}\tau}\}\rangle = \frac{Re\{\mathcal{A}^{*}\mathcal{B}\}}{2}, \tag{3.17}$$

where $\mathcal{A}$ and $\mathcal{B}$ are complex functions and the asterisk denotes a complex conjugate, the function G can be rewritten as

$$G(\xi) = \frac{1}{2}Re\left\{\Pi'^{*}\left(\frac{3W}{1-\varphi\xi} + \frac{\sigma}{12}\Pi\right)\right\}, \tag{3.18}$$

in terms of the reduced leading-order pressure Π and its gradient Π', given respectively in (3.8) and (3.11). Straightforward differentiation of (3.15) yields

$$\frac{\partial\langle P_1\rangle}{\partial\xi} = \frac{(1-\varphi^2)^2}{2(1-\varphi\xi)^3}\int_{-1}^{1} G(\xi)\,\mathrm{d}\xi - G(\xi) \tag{3.19}$$

for the time-averaged pressure gradient. Finally, collecting terms of order ε in (3.4) and taking the time average gives the steady horizontal velocity

$$\langle U_1\rangle = \frac{\partial\langle P_1\rangle}{\partial\xi}\frac{Y(Y-1+\varphi\xi)}{2} - \frac{Y}{4}Re\{\Pi'^{*}W\}, \tag{3.20}$$

where the identity (3.17) has been employed to simplify the second term.

3.3. Non-dimensionalized levitation metrics

Once P_0, $\langle P_1\rangle$ and $\langle U_1\rangle$ are determined, the time-averaged aerodynamic forces and moment can be expressed in the following rescaled forms, each with small asymptotic errors of $O(\varepsilon, h_o/a \sim \theta)$. Using integration by parts, one can rewrite the steady levitation force (2.2) as

$$\langle F_L\rangle = \frac{12\langle\mathcal{F}_L\rangle}{\varepsilon^2\sigma p_a a} = \int_{-1}^{1}\langle P_1\rangle\,\mathrm{d}\xi = -\int_{-1}^{1}\xi\frac{\partial\langle P_1\rangle}{\partial\xi}\,\mathrm{d}\xi, \tag{3.21}$$

and the steady moment about the plate centre (2.4*a*,*b*) as

$$\langle M\rangle = \frac{12\langle\mathcal{M}\rangle}{\varepsilon^2\sigma p_a a^2} = \int_{-1}^{1}\xi\langle P_1\rangle\,\mathrm{d}\xi = -\frac{1}{2}\int_{-1}^{1}\xi^2\frac{\partial\langle P_1\rangle}{\partial\xi}\,\mathrm{d}\xi, \tag{3.22}$$

in terms of the steady pressure gradient. Substituting the definition of the latter, given in (3.19), one may rewrite these expressions as

$$\langle F_L\rangle = \int_{-1}^{1}\xi G(\xi)\,\mathrm{d}\xi - \varphi\int_{-1}^{1}G(\xi)\,\mathrm{d}\xi \tag{3.23}$$

and

$$\langle M\rangle = \left[\frac{1}{2\varphi^2} - 1 + \frac{1}{\varphi}\left(\frac{1-\varphi^2}{2\varphi}\right)^2\ln\left(\frac{1-\varphi}{1+\varphi}\right)\right]\int_{-1}^{1}G(\xi)\,\mathrm{d}\xi + \frac{1}{2}\int_{-1}^{1}\xi^2 G(\xi)\,\mathrm{d}\xi, \tag{3.24}$$

in terms of the known function G (3.18), with the associated dimensionless centre of pressure given by

$$\xi_{csp} = \frac{x_{csp}}{a} = \frac{\langle M\rangle}{\langle F_L\rangle}. \tag{3.25}$$

https://doi.org/10.1017/flo.2023.22 Published online by Cambridge University Press

The thrust force (2.3) can be expressed in the normalized form

$$\langle F_T\rangle = \frac{12\langle \mathcal{F}_T\rangle}{\varepsilon^2\sigma p_a h_o} = \langle F_T\rangle_P + \langle F_T\rangle_S, \tag{3.26}$$

as the sum of the distinct contributions of pressure and shear stress,

$$\langle F_T\rangle_P = \int_{-1}^{1} \varphi\langle P_1\rangle \,\mathrm{d}\xi = \varphi\langle F_L\rangle \quad \text{and} \quad \langle F_T\rangle_S = -\int_{-1}^{1} \frac{\partial\langle U_1\rangle}{\partial Y}\bigg|_{Y=H} \mathrm{d}\xi, \tag{3.27a,b}$$

respectively. Substituting the definition of $\langle U_1\rangle$, given in (3.20), provides

$$\langle F_T\rangle_S = -\frac{\varphi}{2}\langle F_L\rangle - \frac{1}{4}Re\left\{\int_{-1}^{1} \Pi'^{*} W \,\mathrm{d}\xi\right\}, \tag{3.28}$$

where (3.21) has been used in rewriting the first term, which leads to

$$\langle F_T\rangle = \frac{\varphi}{2}\langle F_L\rangle - \frac{1}{4}Re\left\{\int_{-1}^{1} \Pi'^{*} W \,\mathrm{d}\xi\right\} \tag{3.29}$$

for the thrust, upon addition to the first equation in (3.27*a*,*b*). Note that, while the sign of $\langle F_T\rangle_P$ is determined strictly by the direction of levitation, effects of tilt and flexure compete to determine the sign of $\langle F_T\rangle_S$ and, thus, also that of $\langle F_T\rangle$.

3.4. Limiting cases of interest

For SFL systems with non-parallel surfaces undergoing arbitrary flexural oscillations, the integrals required to compute the steady pressure distribution (3.15), levitation force (3.23), moment (3.24) and thrust force (3.29) must be solved numerically. Results for this general problem are presented later, obtained using vectorized global adaptive quadrature (Shampine, 2008) by way of the 'integral' function built into the MATLAB software (MathWorks, 2023).

Discussed below are three special cases that allow analytical determination of the levitation metrics, namely, systems that involve (i) parallel rigid surfaces, (ii) parallel surfaces undergoing a specific class of flexural oscillations and (iii) non-parallel rigid surfaces. Note that these three cases correspond to the simplified levitation systems represented in figures 1(*a*), 1(*b*) and 1(*c*), respectively.

3.4.1. Case I: $\varphi = 0$, $W = 1$

For an SFL system with parallel surfaces that undergo no elastic deformation, i.e. $H(\tau) = 1 + \varepsilon\cos\tau$, the reduced leading-order pressure is given by

$$\Pi(\xi) = \frac{12\,\mathrm{i}}{\beta^2}\left[\frac{\cosh(\beta\xi)}{\cosh\beta} - 1\right], \quad \text{where } \beta = \sqrt{\sigma}\frac{1+\mathrm{i}}{\sqrt{2}}. \tag{3.30}$$

The steady pressure distribution and levitation force are given, respectively, by

$$\langle P_1\rangle(\xi) = \frac{3}{\sigma}\left[5 - \left|\frac{\cosh(\beta\xi)}{\cosh\beta}\right|^2 - 4\,Re\left\{\frac{\cosh(\beta\xi)}{\cosh\beta}\right\}\right] \quad \text{and} \quad \langle F_L\rangle = \frac{30}{\sigma}\left(1 - Re\left\{\frac{\tanh\beta}{\beta}\right\}\right), \tag{3.31a,b}$$

the latter of which is demonstrably identical to the solution found by Minikes et al. (2004).

Due to the lateral symmetry of H (about $\xi = 0$), the thrust and levitation moment vanish, and the centre of steady pressure is correspondingly located at the plate centre, i.e. $\langle F_T\rangle = \langle M\rangle = \xi_{csp} = 0$.

https://doi.org/10.1017/flo.2023.22 Published online by Cambridge University Press

3.4.2. Case II: $\varphi = 0$, $W(\xi) = \sum_i C_i \xi^{n_i} \mathrm{e}^{m_i \xi}$ $\{C_i, m_i \in \mathbb{C}$, $n_i \in \mathbb{Z}_{\geq 0}\}$

For systems with parallel surfaces undergoing flexural oscillation, where $H(\xi, \tau) = 1 + \varepsilon\, Re\{W(\xi)\, \mathrm{e}^{\mathrm{i}\tau}\}$,

$$\Pi(\xi) = \frac{6\,\mathrm{i}}{\beta}\left[L(\xi) - \frac{\sinh[\beta(1+\xi)]}{\sinh(2\beta)} L(1)\right], \quad \text{where } \beta = \sqrt{\sigma}\frac{1+\mathrm{i}}{\sqrt{2}}, \tag{3.32}$$

and the integral function L is defined as

$$L(\xi) = \mathrm{e}^{\beta\xi} \int_{-1}^{\xi} W(\tilde{\xi})\, \mathrm{e}^{-\beta\tilde{\xi}}\, \mathrm{d}\tilde{\xi} - \mathrm{e}^{-\beta\xi} \int_{-1}^{\xi} W(\tilde{\xi})\, \mathrm{e}^{\beta\tilde{\xi}}\, \mathrm{d}\tilde{\xi}. \tag{3.33}$$

The steady pressure distribution is then given by

$$\langle P_1 \rangle(\xi) = \frac{1+\xi}{2} \int_{-1}^{1} G(\xi)\, \mathrm{d}\xi - \int_{-1}^{\xi} G(\tilde{\xi})\, \mathrm{d}\tilde{\xi}, \quad \text{where } G = \frac{1}{2} Re\left\{\Pi'^{*}\left(3W + \frac{\sigma}{12}\Pi\right)\right\}, \tag{3.34}$$

and the levitation force and moment are defined, respectively, by the simplified integrals

$$\langle F_L \rangle = \int_{-1}^{1} \xi G(\xi)\, \mathrm{d}\xi \quad \text{and} \quad \langle M \rangle = \frac{1}{2}\int_{-1}^{1} \xi^2 G(\xi)\, \mathrm{d}\xi - \frac{1}{6}\int_{-1}^{1} G(\xi)\, \mathrm{d}\xi. \tag{3.35a,b}$$

First-order corrections to the pressure give no contribution to the thrust force due to the absence of tilt ($\varphi = 0$), whereby $\langle F_T \rangle_P = 0$ and $\langle F_T \rangle_S = \langle F_T \rangle = -(1/4)\, Re\{\int_{-1}^{1} \Pi'^{*}(\xi) W(\xi)\, \mathrm{d}\xi\}$.

In their asymptotic study, Minikes et al. (2004) computed $\langle F_T \rangle$ analytically for the case of pure travelling-wave oscillations, and utilized finite-difference methods for computing first-order pressure corrections. The generalized formulation above allows integral expression of the thrust, as well as the accompanying levitation force and moment, for arbitrary waveforms $W(\xi)$. Fully analytical computation is possible for waves of the type $W(\xi) = \sum_i C_i \xi^{n_i} \mathrm{e}^{m_i \xi}$, where each C_i and m_i are complex numbers and each n_i is a whole number, which allow explicit integration in (3.33)–(3.35*a*,*b*). Such waves can be found, for instance, as solutions to the Euler–Bernoulli equation, which governs the dynamic bending of beams (Geist & McLaughlin, 1994; Yang, 2005).

3.4.3. Case III: $\varphi \neq 0$, $W = 1$

For rigid-body systems with non-parallel surfaces, where $W = 1$ and $H(\xi, \tau) = 1 - \varphi\xi + \varepsilon \cos\tau$, the reduced leading-order pressure assumes the form

$$\Pi(\xi) = \frac{12\,\mathrm{i}}{\varphi^2\alpha^2} \frac{1}{1-\varphi\xi}\left[\frac{(1-\varphi^2)^{\alpha}(1-\varphi\xi)^{-\alpha} + (1-\varphi\xi)^{\alpha}}{(1+\varphi)^{\alpha} + (1-\varphi)^{\alpha}} - 1\right], \tag{3.36}$$

with α defined in (3.9). Analytical expressions for the steady levitation metrics can be found through tedious but straightforward algebra. Most notably, the contribution of shear stress to the thrust force is opposite in direction and half in magnitude to that of film pressure. This can be shown simply by substituting $W = 1$ into (3.28), which gives $\langle F_T \rangle_S = -\varphi \langle F_L \rangle/2 = -\langle F_T \rangle_P/2$.

Of practical interest is the behaviour of the solution when the film thickness is severely reduced and, thus, the greatest repulsive levitation forces are expected to occur (Zhao, 2010). In the associated limit $\sigma \to \infty$, the steady overpressure distribution simplifies to $\langle P_1 \rangle(\xi) = 15/[\sigma(1-\varphi\xi)^2]$, not accounting for the rapid relaxation of $\langle P_1 \rangle$ to zero at the edges of the film $\xi = \pm 1$ (DiPrima, 1968). The corresponding levitation force and moment assume the simplified forms

$$\lim_{\sigma\to\infty} \langle F_L \rangle = \frac{30}{\sigma(1-\varphi^2)} \quad \text{and} \quad \lim_{\sigma\to\infty} \langle M \rangle = \frac{15}{\sigma\varphi^2}\left[\ln\left(\frac{1-\varphi}{1+\varphi}\right) + \frac{2\varphi}{1-\varphi^2}\right]. \tag{3.37a,b}$$

https://doi.org/10.1017/flo.2023.22 Published online by Cambridge University Press

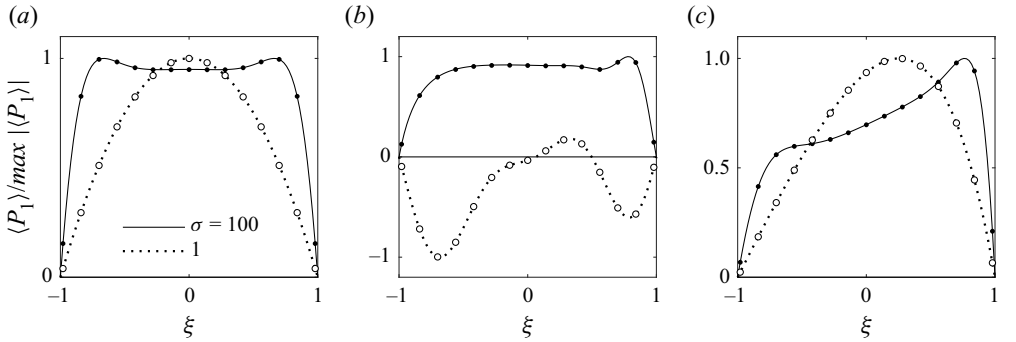

Figure 4. *Sample profiles of the normalized time-averaged film pressure for SFL systems with (a) zero flexure and zero tilt, (b) pure travelling-wave flexure and (c) non-zero tilt. Asymptotic results (continuous and dotted curves) are verified with numerical solutions of* (2.11) *for* $\varepsilon = 0.01$ *(dots and circles). Results are shown for (a)* $W = 1, \varphi = 0$*, (b)* $W = \exp(-2i\pi\xi), \varphi = 0$ *and (c)* $W = 1, \varphi = 0.2$*.*

4. Discussion of results

4.1. Time-averaged squeeze-film pressure

Exemplified in figure 4 are normalized distributions of the time-averaged first-order pressure $\langle P_1\rangle(\xi)$ for the three limiting cases discussed above and represented in figure 1(*a–c*): (*a*) rigid bodies with parallel surfaces, (*b*) parallel surfaces with travelling-wave oscillations $W = \exp(-2\,\mathrm{i}\pi\xi)$ and (*c*) rigid bodies with a surface tilt ratio of $\varphi = \theta/(h_o/a) = 0.2$. For all three cases displayed, $\langle P_1\rangle(\xi)$ depends strongly on the squeeze number $\sigma = 12\mu_a\omega a^2/(p_a h_o^2)$. In particular, when $\sigma \gg 1$ and effects of gaseous compressibility are correspondingly augmented, as discussed below (2.5), the overpressure varies gradually within the film and relaxes sharply near its edges, in agreement with prior results (DiPrima, 1968; Ramanarayanan et al., 2022; Salbu, 1964).

For a flexible plate undergoing travelling-wave deformations, the steady overpressure distribution becomes largely negative for critically small values of σ, in agreement with prior results that demonstrate a strong correlation between flexural oscillations and the emergence of suction forces in SFL systems (Ramanarayanan & Sánchez, 2022). It is of interest to understand the behaviours of such systems because of their potential to provide controlled transport with attractive levitation, a phenomenon that is yet to be demonstrated with rigorous experimentation.

For a rigid plate with a positive inclination angle, the steady pressure distribution is skewed such that $\langle P_1\rangle$ assumes larger values near the lowered leading edge $\xi = 1$. Correspondingly, while the steady film pressure yields a positive contribution $\varphi\langle F_L\rangle$ to the thrust, the steady shear force caused by first-order streaming acts in the opposite direction, reducing $\langle F_T\rangle$ by a factor of two, as noted below (3.36).

4.2. Visualization of levitation metrics

In pursuit of a practical understanding of the generic SFL transport system outlined in figure 3, it is of interest to delineate clearly – i.e. in a manner amenable to physical interpretation – the parametric dependences of the steady levitation metrics on the tilt ratio $\varphi = \theta/(h_o/a)$, flexural waveform $W(\xi)$ and squeeze number $\sigma = 12\mu_a\omega a^2/(p_a h_o^2)$.

Although these three governing parameters are considered to be 'independent' under the present formulation, variations in σ can, in practice, affect W. In particular, since SFL oscillators typically operate near resonance (Ilssar et al., 2017), altering their excitation frequency ω or length $2a$ may disturb substantially the amplitude b and wavelength of their flexural deformations. Therefore, it seems most appropriate to interpret the variation with σ of the levitation forces and moment as a variation with the levitation height h_o. The latter is typically a 'dependent' variable that responds freely to changes in

https://doi.org/10.1017/flo.2023.22 Published online by Cambridge University Press

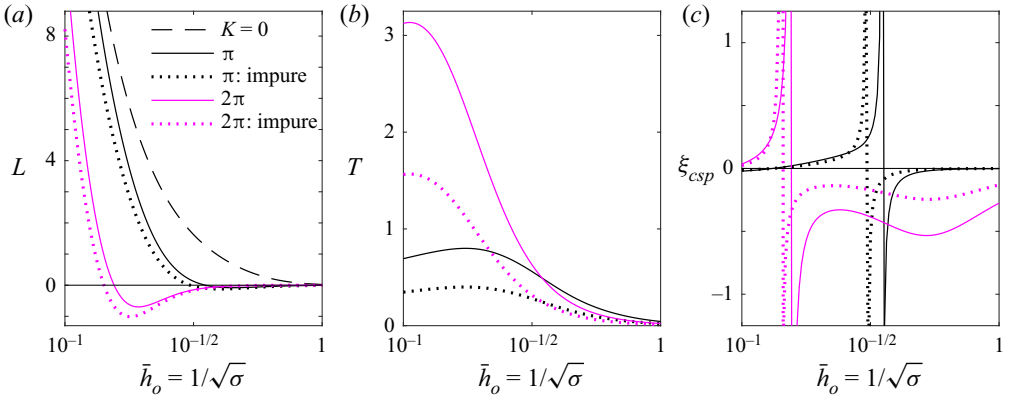

Figure 5. *Variation with the normalized levitation height* $\bar{h}_o$ (4.2) *of the dimensionless (a) levitation and (b) thrust forces* (4.1*a*,*b*) *and (c) the centre of steady pressure* (3.25)*, for a travelling-wave-driven system with varying wavenumber K. Curves labelled 'impure' are computed for a wave purity of* $\mathcal{P} = 0.5$ (4.3).

the load $\langle \mathcal{F}_L \rangle$, for instance, the change in apparent weight of a mobile robot as it travels along a curved path as in figure 2(*b*) (Weston-Dawkes et al., 2021). (Note that, for oscillators with sufficiently low mass or flexural rigidity, *b* and *W* may be affected significantly by variations in h_o and the tilt angle θ (Ilssar & Bucher, 2017; Weston-Dawkes et al., 2021); such coupled interactions are not considered below.)

Correspondingly, in representing the present asymptotic results, it is convenient to renormalize the steady levitation and thrust forces according to

$$L = \left(\frac{\sigma}{12}\right)^2 \langle F_L \rangle = \frac{\langle \mathcal{F}_L \rangle}{b^2 p_a^2/(\mu_a \omega a)} \quad \text{and} \quad T = \left(\frac{\sigma}{12}\right)^{3/2} \langle F_T \rangle = \frac{\langle \mathcal{F}_T \rangle}{b^2 p_a^{3/2}/(a\sqrt{\mu_a \omega})}, \tag{4.1a,b}$$

where multiplication by an appropriate power of σ has eliminated h_o. Upon introducing also a normalized height

$$\bar{h}_o = \frac{1}{\sqrt{\sigma}} = \frac{h_o}{2a\sqrt{3\mu_a \omega/p_a}}, \tag{4.2}$$

the dimensionless functions $L(\bar{h}_o)$ and $T(\bar{h}_o)$ can be interpreted to represent the variations of the levitation and thrust forces with the mean levitation height, for a given tilt ratio and flexural mode.

Displayed in figures 5 and 6 are the variations with $\bar{h}_o$ of *L*, *T* and the centre of steady pressure ξ_{csp} for the canonical transport systems pictured in figures 1(*b*) and 1(*c*), respectively. It may be readily noted from both figures that the limiting behaviours of *L* for small and large values of $\bar{h}_o = 1/\sqrt{\sigma}$ are consistent with prior knowledge concerning the role of gaseous compressibility in SFL systems, the latter elucidated below (2.5). The behaviour of the solution for intermediate levitation heights $\bar{h}_o \sim 1$, however, differs substantially between the two cases and will be discussed below.

4.3. Transport by travelling-wave oscillations

The solid curves in figure 5 represent the levitation metrics for systems with parallel surfaces ($\varphi = 0$) driven by pure travelling waves $W = \mathrm{e}^{-\mathrm{i}K\xi}$, where *K* is the relevant dimensionless wavenumber that has been normalized with the inverse of the semi-length *a*.

As seen respectively in panels (*a*) and (*b*), the levitation force is significantly reduced by flexure within the displayed range of heights $\bar{h}_o$, and the thrust force exhibits a finite maximum at a critical height that varies with *K*. Investigation of the limit $\bar{h}_o \to 0$ (or, equivalently, $\sigma \to \infty$) reveals that curves of *L* for all values of *K* eventually converge in the case of pure travelling waves, in agreement

https://doi.org/10.1017/flo.2023.22 Published online by Cambridge University Press

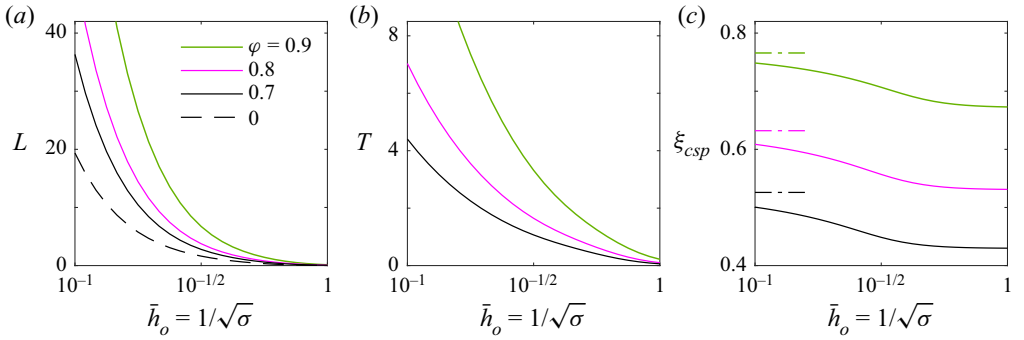

Figure 6. *Variation with the normalized levitation height $\bar{h}_o$ of the dimensionless (a) levitation and (b) thrust forces and (c) the centre of steady pressure ξ_{csp} for a rigid-body SFL system, for various values of the tilt ratio φ (2.7). Limiting values of ξ_{csp} for $\bar{h}_o \to 0$ (broken lines) are found using (3.25) and (3.37a,b).*

with the findings of Minikes et al. (2004), who noted that optimization of these systems for repulsive operation warrants compromising between a levitation force that increases for decreasing values of $\bar{h}_o$ and a thrust force that varies non-monotonically.

Furthermore, as seen in figure 5(*c*), the centre of pressure varies strongly with $\bar{h}_o$, indicative of a non-negligible sensitivity to levitation height that must be taken into account when designing and controlling a mobile robot or a rail-transport system. Interestingly, ξ_{csp} exhibits a singularity at a critical height that corresponds to a state of zero levitation. Beyond this critical height, L assumes negative values, corresponding to attractive levitation (see the associated distribution of steady film pressure exemplified in figure 4*c*). Both the attractive load capacity and the maximum thrust rise with increasing values of the wavenumber K.

As noted previously, generation of pure travelling-wave deformations of a finite body is hindered by the reflection of propagating waves at open boundaries and points of actuation. The resulting impure travelling waves can be modelled approximately with use of the modified waveform

$$W = \cos(K\xi) - \mathrm{i}\mathcal{P}\sin(K\xi), \quad \text{with } 0 \le \mathcal{P} \le 1, \tag{4.3}$$

where $\mathcal{P}$ constitutes a coefficient of purity. Namely, when $\mathcal{P} = 1$, W parametrizes the classical travelling wave $\mathrm{e}^{-\mathrm{i}K\xi}$, and when $\mathcal{P} = 0$, a perfect standing wave of equal wavenumber and amplitude (Feng et al., 2015; Minikes & Bucher, 2003). Note that the inverse of $\mathcal{P}$ is often referred to in literature as the 'standing-wave ratio'. As exemplified by the dotted curves in figures 5(*a*) and 5(*b*), introduction of impurity in a travelling-wave-driven SFL system seems to improve the attractive load capacity, but reduces drastically the maximum thrust force that can be produced.

4.4. Effects of surface inclination

Represented in figure 6 are the levitation metrics for a rigid-body system ($W = 1$) with various tilt ratios $\varphi = \theta/(h_o/a)$. Recall that φ is a dimensionless representation of the amount of tilt where, for any given levitation height h_o, $\varphi = 0$ denotes parallel surfaces and $\varphi = \pm(1 - \varepsilon)$ denotes maximum tilt in either direction – i.e. the leading or trailing edge of the plate comes into contact with the wall during each downward stroke of the oscillation cycle.

It is clear from figures 6(*a*) and 6(*b*) that tilting the plate about its centre substantially increases the levitation and thrust forces at any given operating height $\bar{h}_o$. Both appear to increase unboundedly as $\bar{h}_o \to 0$, assuming substantially greater values than those produced by flexure-driven systems, for the range of $\bar{h}_o$ displayed. Indeed, in the associated limit of large σ (3.37*a*,*b*), L becomes proportional to

https://doi.org/10.1017/flo.2023.22 Published online by Cambridge University Press

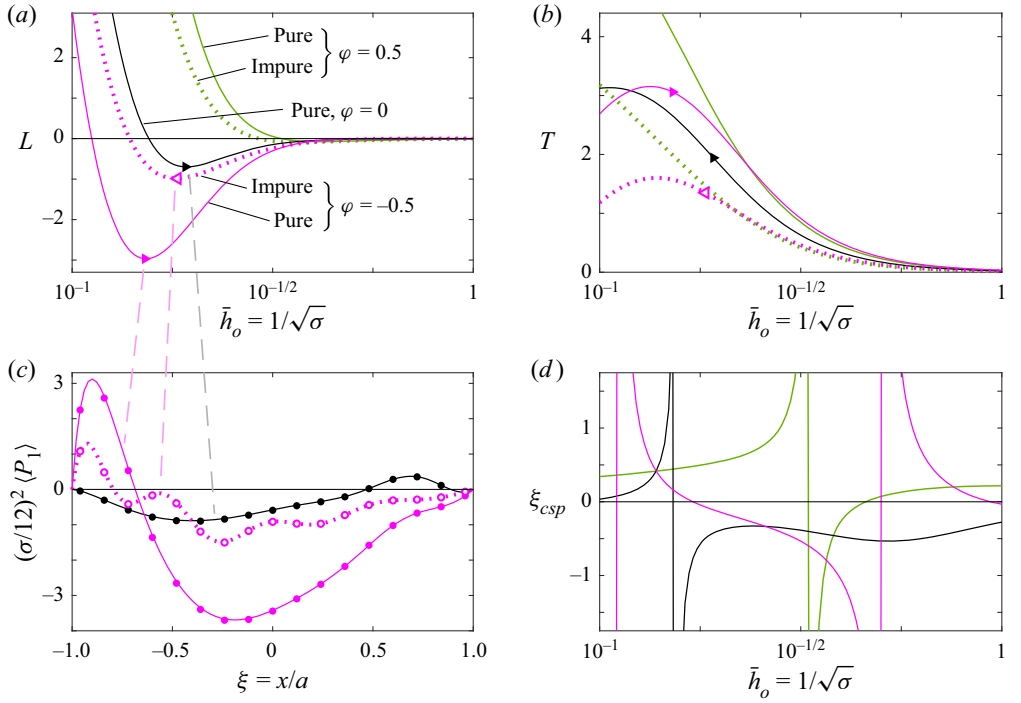

Figure 7. *Variation with the normalized levitation height $\bar{h}_o$ (4.2) of the rescaled (a) levitation force (4.1a,b), (b) thrust and (d) centre of steady pressure (3.25), for a flexural system with wavenumber $K = 2\pi$. Curves are shown for various tilt ratios φ (2.7) and wave purities $\mathcal{P}$ (4.3); curves labelled 'impure' are computed for $\mathcal{P} = 0.5$. Plotted in (c), and verified numerically for $\varepsilon = 0.01$ (dots and circles), are profiles of steady pressure for states where the system produces maximal attraction, marked with triangles in (a) and (b).*

the inverse square of the levitation height $\bar{h}_o^{-2}$, well in agreement with prior research (Taylor & Saffman, 1957), and $T \propto \bar{h}_o^{-1}$. Of course, both are physically limited since h_o cannot decrease below the amplitude b (Zhao, 2010). Finally, figure 6(*c*) demonstrates that the centre of steady pressure moves toward the leading edge with increasing tilt and varies rather weakly with $\bar{h}_o$. The associated steady moment acts to reduce the angle of inclination, in agreement with the findings of Li et al. (2017).

One may anticipate that these effects of surface inclination apply also to systems with non-uniform oscillations, for which $\mathrm{d}W/\mathrm{d}\xi \neq 0$. Firstly, the sensitivity of ξ_{csp} to perturbations in levitation height can be expected to increase with the onset of flexure near resonance, accompanying a possible transition to attractive levitation forces (Ramanarayanan & Sánchez, 2022). For systems with lateral symmetry, where $W(-\xi) = W(\xi)$ for $0 < \xi \leq 1$, inclination in either direction is expected to (i) provide significant thrust and (ii) increase substantially the existing repulsive levitation force. Systems undergoing asymmetrical oscillations require further investigation.

Visualized using solid curves in figure 7, for example, are the levitation metrics of a system driven by pure travelling waves, for various values of the tilt ratio φ. As seen in panel (*a*), positive and negative inclination increase substantially the repulsive and attractive load capacities, respectively. The aptly rescaled steady pressure distributions that correspond to the state of maximal attraction are compared in panel (*c*) for $\varphi = \theta/(h_o/a) = 0$ and -0.5. Panel (*b*) reveals that inclination in either direction increases also the thrust force T for a wide range of levitation heights $\bar{h}_o$, due to the combined contributions of fluid shear (stemming from wave propagation) and pressure (from surface tilt). The dotted curves in panels (*a–c*) indicate, however, that the degree of purity of the travelling wave significantly impacts the extent to which these benefits may be realized practically. Panel (*d*), where only pure travelling waves are

https://doi.org/10.1017/flo.2023.22 Published online by Cambridge University Press

considered for purposes of visual clarity, confirms the high variability of the centre of steady pressure that accompanies the transition from repulsion to attraction for flexural systems.

4.5. Optimization of travelling-wave-driven systems with variable inclination

Based on the preliminary results above, it appears that incorporating the mechanism of controlled inclination may improve the effectiveness of transport systems driven by impure travelling-wave oscillations for purposes of both repulsive and attractive SFL. To quantify precisely the extent of improvement that may be gained, we conclude this paper with a rigorous investigation of the associated generalized problem.

As discussed in § 1, the purity $\mathcal{P}$ of a travelling wave is limited by the effectiveness of the wave-generation method, and the wavenumber K is typically determined by the chosen natural frequency and geometric properties of the oscillator. Active feedback control is often employed to ensure that the resulting waveform W remains constant during operation. In contrast, the levitation height $\bar{h}_o$ and tilt ratio φ are free to respond to (i) perturbation by external forces and/or (ii) active adjustments to the mass or centre of mass of the levitated object. In pursuit of quantifying the maximal capabilities of travelling-wave-driven SFL systems that feature controllable inclination, we therefore explore the parametric domain spanned by $\bar{h}_o$ and φ, for a fixed wavenumber $K = 2\pi$ and select values of $\mathcal{P}$.

Two important distinctions must be drawn at this point between the mobile robot depicted in figure 2(*b*) and the rail-transport system schematized in figure 2(*a*). In the case of the former, the oscillator is attached to the levitated object, such that the waveform W is invariant as the object travels. In contrast, for rail-transport systems, the wave is subject to a phase shift that evolves as the object translates, whereby stationary components in the wave can cause fluctuations in the levitation forces and moment. The resulting operational instabilities may be especially pronounced for travelling waves with lower purity $\mathcal{P}$ and relative wavenumber K (Hashimoto, Koike, & Ueha, 1996; Liang, Ling, & Zhang, 2010; Sadayuki, 2002). Secondly, the mass distribution of a self-levitating mobile robot may be adjusted actively to control the inclination φ, but that of a levitated object in a rail-transport system is typically fixed. Both of these distinctions must be considered carefully when interpreting and applying practically the following results.

The performance objective(s) for an SFL system will vary with the desired transportation path, for instance, translation (i) above a horizontal surface, (ii) below a horizontal surface, (iii) upward or downward along a vertical surface or otherwise (see figure 2 for clarificatory illustrations).

For transport above a horizontal surface, possible objectives include maximizing the repulsive levitation force L and/or the thrust T. Based on the results outlined in figures 5–7, L and T may be maximized by increasing the positive tilt angle and the wave purity, respectively, as much as physically possible.

For transport below a horizontal surface, it may be of interest to maximize the attractive levitation force $(-L)$ and/or the thrust T. As seen, for example, in figures 5 and 7, L may exhibit a negative global minimum for a critical levitation height $\bar{h}_o = \bar{h}_o^*$. Plotted in figure 8 are the non-monotonic variations with φ of this maximal attractive force $L(\bar{h}_o^*)$ and the corresponding thrust $T(\bar{h}_o^*)$ for various values of $\mathcal{P}$, demonstrating that there is a critical range of tilt ratios for which the performance of such a system is maximized. For instance, when $\mathcal{P} = 0.5$, an inclination of $-0.4 \lessapprox \varphi \lessapprox -0.25$ is most desirable. Note that the benefits of controlled inclination are greater for purer travelling waves. Of practical concern is the fact that systems operating at this critical height are unstable to positive perturbations in $\bar{h}_o$ – that is, $\partial L/\partial \bar{h}_o > 0$ for $\bar{h}_o > \bar{h}_o^*$. For this reason, operating below the maximum capacity, at a height $\bar{h}_o < \bar{h}_o^*$, is recommended for avoiding catastrophic failure during attractive levitation.

Finally, for vertical transport along an upright surface, the thrust force must be maximized while the levitation force L must be identically zero. As seen, for example, in figures 5 and 7, the function $L(\bar{h}_o)$ may vanish at a critical height $\bar{h}_o'$, corresponding to a transition from repulsive to attractive levitation. A system that operates at this height is necessarily stable to positive and negative perturbations in $\bar{h}_o$ – i.e. $\partial L/\partial \bar{h}_o < 0$ for $\bar{h}_o = \bar{h}_o'$. Plotted in figure 9 is the variation with the tilt ratio φ of the

https://doi.org/10.1017/flo.2023.22 Published online by Cambridge University Press

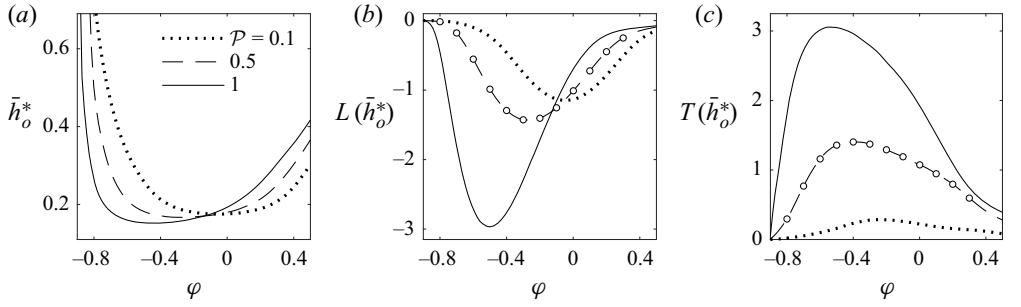

Figure 8. *Variation with the tilt ratio φ of (a) the normalized critical levitation height at which a travelling-wave-driven system with wavenumber $K = 2\pi$ generates maximal attraction, and the corresponding values of (b) the levitation force L and (c) the thrust T, for three values of the wave purity $\mathcal{P}$ (4.3). For the case $\mathcal{P} = 0.5$, L and T are verified with numerical solutions computed for $\varepsilon = 0.01$ (circles).*

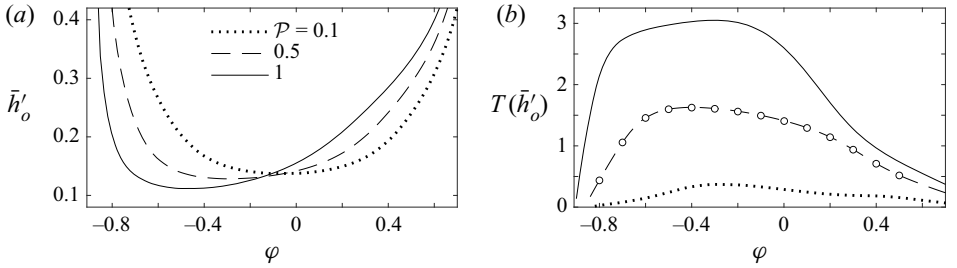

Figure 9. *Variation with the tilt ratio φ of (a) the normalized critical levitation height at which a travelling-wave-driven system with wavenumber $K = 2\pi$ generates zero levitation force and (b) the corresponding value of the thrust force T, for three values of the wave purity $\mathcal{P}$ (4.3). For the case $\mathcal{P} = 0.5$, asymptotic results for T are verified with numerical solutions computed for $\varepsilon = 0.01$ (circles).*

corresponding thrust force $T(\bar{h}_o')$ for various values of the wave purity $\mathcal{P}$. Once again, there appears to be a desirable range of tilt ratios for which performance is maximized, with greater benefits obtained for purer oscillations.

These analyses may be readily extended to address more complex design problems, those that may require inclined transport paths and involve performance criteria that concern simultaneously the levitation force $\langle \mathcal{F}_L \rangle$, thrust $\langle \mathcal{F}_T \rangle$ and stability to perturbations in the tilt angle θ.

5. Conclusions

Developed in this paper is a theoretical description of the planar, viscous, compressible airflow in contactless transport systems that operate using SFL. The reduced asymptotic formulation, which accounts for non-uniform structural oscillations of non-parallel surfaces, provides fundamental insights into the fluidic mechanisms that underlie thrust generation in squeeze-film systems, and enables rapid computation of their performance characteristics using integral expressions.

Particular attention is dedicated to studying the influence of surface inclination on transport systems that are driven by impure travelling waves (see figures 2 and 3). Results demonstrate that controlled modulation of the tilting angle can improve substantially the maximum achievable thrust as well as the load capacity for systems that operate using both repulsive and attractive levitation. In the case of the latter, the amount of improvement that can be gained depends strongly on the purity of the travelling wave, or more generally, presumably on the degree of lateral asymmetry in the flexural oscillations.

Sample computations are provided to display the potential of the present formulation in serving as an efficient tool to supplement the design, optimization and active control of mobile robots. The accuracy

https://doi.org/10.1017/flo.2023.22 Published online by Cambridge University Press

and versatility of this theoretical model must be improved in the future by modelling appropriately the effects of non-negligible transport speeds (DiPrima, 1968), free vibrations of the levitated object (Ilssar & Bucher, 2017; Yoshimoto, 1997), fluid–structure coupling by which the flexural waveform of the oscillator may alter in response to changes in levitation height and tilt angle (Weston-Dawkes et al., 2021), fluid inertia and the accompanying relaxation of steady pressure beyond the boundaries of the squeeze film (Ramanarayanan et al., 2022) and surface roughness, which can substantially reduce the levitation force and transport speed (Chen et al., 2016; Weston-Dawkes et al., 2021).

Acknowlegements. We gratefully acknowledge insightful conversations with Dr Tolley and Mr Chengze-Jia regarding the practical applicability of transport using attractive SFL.

Declaration of interests. The authors declare no conflict of interest.

References

Andrade, M.A.B., Ramos, T.S., Adamowski, J.C., & Marzo, A. (2020). Contactless pick-and-place of millimetric objects using inverted near-field acoustic levitation. *Applied Physics Letters*, *116*(5), 054104.

Chapman, S., & Cowling, T.G. (1990). *The mathematical theory of non-uniform gases: An account of the kinetic theory of viscosity, thermal conduction and diffusion in gases*. Cambridge, UK: Cambridge University Press.

Chen, K., Gao, S., Pan, Y., & Guo, P. (2016). Self-running and self-floating two-dimensional actuator using near-field acoustic levitation. *Applied Physics Letters*, *109*(12), 123503.

Colasante, D.A. (2015, March). Apparatus and method for orthosonic lift by deflection. *U.S. Patent No. 08967965 B1*. Washington, DC: U.S. Patent and Trademark Office. https://patentscope.wipo.int/search/en/detail.jsf?docId=US130909010

DiPrima, R.C. (1968). Asymptotic methods for an infinitely long slider squeeze-film bearing. *Journal of Lubrication Technology*, *90*, 173–183.

Feng, K., Liu, Y., & Cheng, M. (2015). Numerical analysis of the transportation characteristics of a self-running sliding stage based on near-field acoustic levitation. *The Journal of the Acoustical Society of America*, *138*(6), 3723–3732.

Geist, B., & McLaughlin, J. (1994). The effect of structural damping on nodes for the Euler-Bernoulli beam: A specific case study. *Applied Mathematics Letters*, *7*(3), 51–55.

Ghenna, S., Giraud, F., Giraud-Audine, C., Amberg, M., & Lemaire-Semail, B. (2015). Modelling and control of a travelling wave in a finite beam, using multi-modal approach and vector control method. In *2015 joint conference of the IEEE international frequency control symposium & the European frequency and time forum* (pp. 509–514). IEEE.

Giraud, F., Giraud-Audine, C., Amberg, M., & Lemaire-Semail, B. (2014). Vector control method applied to a traveling wave in a finite beam. *IEEE Transactions on Ultrasonics, Ferroelectrics, and Frequency Control*, *61*(1), 147–158.

Hariri, H., Bernard, Y., & Razek, A. (2013). A traveling wave piezoelectric beam robot. *Smart Materials and Structures*, *23*(2), 025013.

Hashimoto, Y., Koike, Y., & Ueha, S. (1996). Near-field acoustic levitation of planar specimens using flexural vibration. *The Journal of the Acoustical Society of America*, *100*(4), 2057–2061.

Hatanaka, T., Koike, Y., Nakamura, K., Ueha, S., & Hashimoto, Y. (1999). Characteristics of underwater near-field acoustic radiation force acting on a planar object. *Japanese Journal of Applied Physics*, *38*(11A), L1284.

Ide, T., Friend, J., Nakamura, K., & Ueha, S. (2007). A non-contact linear bearing and actuator via ultrasonic levitation. *Sensors and Actuators A: Physical*, *135*(2), 740–747.

Ilssar, D., & Bucher, I. (2017). The effect of acoustically levitated objects on the dynamics of ultrasonic actuators. *Journal of Applied Physics*, *121*(11), 114504.

Ilssar, D., Bucher, I., & Flashner, H. (2017). Modeling and closed loop control of near-field acoustically levitated objects. *Mechanical Systems and Signal Processing*, *85*, 367–381.

Koyama, D., Nakamura, K., & Ueha, S. (2007). A stator for a self-running, ultrasonically-levitated sliding stage. *IEEE Transactions on Ultrasonics, Ferroelectrics, and Frequency Control*, *54*(11), 2337–2343.

Lagerstrom, P.A. (1988). *Matched asymptotic expansions: Ideas and techniques*. New York, NY: Springer-Verlag.

Langlois, W. (1962). Isothermal squeeze films. *Quarterly of Applied Mathematics*, *20*(2), 131–150.

Li, J., Cao, W., Liu, P., & Ding, H. (2010). Influence of gas inertia and edge effect on squeeze film in near field acoustic levitation. *Applied Physics Letters*, *96*(24), 243507.

Li, J., Liu, C., & Zhang, W. (2017). Pressure potential and stability analysis in an acoustical noncontact transportation. *Acoustical Physics*, *63*, 125–131.

Li, J., Liu, P., & Ding, H. (2014). Dynamic coupling and experimental study on flexural transducer used in near field acoustic levitation. *Journal of Advanced Mechanical Design, Systems, and Manufacturing*, *8*(3), JAMDSM0038.

Liang, Y.D., Ling, H., & Zhang, Y. (2010). Study on the conditions of near-field acoustic levitation. In *Advanced Materials Research: Vol. 97. Manufacturing science and engineering I* (pp. 4135–4140). Trans Tech Publications Ltd.

Loh, B.G., & Ro, P.I. (2000). An object transport system using flexural ultrasonic progressive waves generated by two-mode excitation. *IEEE Transactions on Ultrasonics, Ferroelectrics, and Frequency Control*, *47*(4), 994–999.

https://doi.org/10.1017/flo.2023.22 Published online by Cambridge University Press

MathWorks. (2023). *Numerical integration and differentiation*. https://www.mathworks.com/help/matlab/ref/integral.html

Matsuo, E., Koike, Y., Nakamura, K., Ueha, S., & Hashimoto, Y. (2000). Holding characteristics of planar objects suspended by near-field acoustic levitation. *Ultrasonics*, *38*(1–8), 60–63.

Melikhov, I., Chivilikhin, S., Amosov, A., & Jeanson, R. (2016). Viscoacoustic model for near-field ultrasonic levitation. *Physical Review E*, *94*(5), 053103.

Michael, W.A. (1963). Approximate methods for time-dependent gas-film lubrication problems. *Journal of Applied Mechanics*, *30*(4), 509–517.

Minikes, A., & Bucher, I. (2003). Noncontacting lateral transportation using gas squeeze film generated by flexural traveling waves–numerical analysis. *The Journal of the Acoustical Society of America*, *113*(5), 2464–2473.

Minikes, A., & Bucher, I. (2006). Comparing numerical and analytical solutions for squeeze-film levitation force. *Journal of Fluids and Structures*, *22*(5), 713–719. https://www.sciencedirect.com/science/article/pii/S088997460600017X.

Minikes, A., Bucher, I., & Haber, S. (2004). Levitation force induced by pressure radiation in gas squeeze films. *The Journal of the Acoustical Society of America*, *116*(1), 217–226.

Ramanarayanan, S., Coenen, W., & Sánchez, A.L. (2022). Viscoacoustic squeeze-film force on a rigid disk undergoing small axial oscillations. *Journal of Fluid Mechanics*, *933*, A15.

Ramanarayanan, S., & Sánchez, A.L. (2022). On the enhanced attractive load capacity of resonant flexural squeeze-film levitators. *AIP Advances*, *12*(10), 105126.

Sadayuki, U. (2002). Phenomena, theory and applications of near-field acoustic levitation. *Rev Acoustic*, *33*(3–4), 21.

Salbu, E. (1964). Compressible squeeze films and squeeze bearings. *Journal of Basic Engineering*, *86*(2), 355–364.

Shampine, L.F. (2008). Vectorized adaptive quadrature in MATLAB. *Journal of Computational and Applied Mathematics*, *211*(2), 131–140.

Shi, M., An, L., Feng, K., Guo, Z., & Liu, W. (2018). Numerical and experimental study on the influence of material characteristics on the levitation performance of squeeze-film air bearing. *Tribology International*, *126*, 307–316.

Shi, M., Feng, K., Hu, J., Zhu, J., & Cui, H. (2019). Near-field acoustic levitation and applications to bearings: A critical review. *International Journal of Extreme Manufacturing*, *1*(3), 032002.

Stolarski, T., Gawarkiewicz, R., & Tesch, K. (2015). Acoustic journal bearing–a search for adequate configuration. *Tribology International*, *92*, 387–394.

Syuhri, S.N.H. (2022). *Fluid flow induced by travelling waves in beam-like structures: Modelling, simulation and experimental validation* (Unpublished doctoral dissertation). Glasgow, UK: University of Glasgow.

Takasaki, M., Terada, D., Kato, Y., Ishino, Y., & Mizuno, T. (2010). Non-contact ultrasonic support of minute objects. *Physics Procedia*, *3*(1), 1059–1065.

Taylor, S.G., & Saffman, P. (1957). Effects of compressibility at low Reynolds number. *Journal of the Aeronautical Sciences*, *24*(8), 553–562.

Tomikawa, Y., Adachi, K., Hirata, H., Suzuki, T., & Takano, T. (1990). Excitation of a progressive wave in a flexurally vibrating transmission medium. *Japanese Journal of Applied Physics*, *29*(S1), 179.

Wang, C., & Au, Y.J. (2013). Comparative performance of squeeze film air journal bearings made of aluminium and copper. *The International Journal of Advanced Manufacturing Technology*, *65*, 57–66.

Wei, B., Shaham, R., & Bucher, I. (2018). Theoretical investigation and prototype design for non-parallel squeeze film movement platform driven by standing waves. *Tribology International*, *119*, 539–548.

Weston-Dawkes, W.P., Adibnazari, I., Hu, Y.W., Everman, M., Gravish, N., & Tolley, M.T. (2021). Gas-lubricated vibration-based adhesion for robotics. *Advanced Intelligent Systems*, *3*(7), 2100001.

Yang, B. (2005). Free vibration of membranes and plates. In *Stress, strain, and structural dynamics* (pp. 807–851). Burlington, VT: Academic Press.

Yano, R., Aoyagi, M., Tamura, H., & Takano, T. (2011). Novel transfer method using near-field acoustic levitation and its application. *Japanese Journal of Applied Physics*, *50*(7S), 07HE29.

Yin, Y. (2008). *Non-contact object transportation using near-field acoustic levitation induced by ultrasonic flexural waves* (Unpublished doctoral dissertation). Raleigh, NC: North Carolina State Univeristy.

Yoshimoto, S. (1997). Floating characteristics of squeeze-film gas bearings with vibration absorber for linear motion guide. *Journal of Lubrication Technology*, *119*, 531–536.

Yoshimoto, S., Shou, T., & Somaya, K. (2013). Vertical attractive force generated in a noncontact chuck using ultrasonic vibration. *Precision Engineering*, *37*(4), 805–811.

Zhao, S. (2010). *Investigation of non-contact bearing systems based on ultrasonic levitation* (Unpublished doctoral dissertation). Paderborn, Germany: Paderborn University.

Cite this article: Ramanarayanan S, Sánchez AL (2023). Benefits of controlled inclination for contactless transport by squeeze-film levitation. *Flow*, *3*, E26. doi:10.1017/flo.2023.22